

Directed Percolation in Temporal Networks

Arash Badie-Modiri,¹ Abbas K. Rizi,¹ Márton Karsai,^{2,3} and Mikko Kivelä¹

¹*Department of Computer Science, School of Science, Aalto University, FI-0007, Finland*

²*Department of Network and Data Science Central European University, 1100 Vienna, Austria*

³*Alfréd Rényi Institute of Mathematics, 1053 Budapest, Hungary*

(Dated: April 6, 2024)

Connectivity transitions in static networks are well described by percolation theory, yet the corresponding description is not developed for temporal networks. We map the connectivity problem of temporal networks to directed percolation and show that the reachability phase transition in random temporal network models, as induced by any limited-waiting-time process, appears with the mean-field exponents of directed percolation. Furthermore, we measure the central thermodynamic quantities adapted to large-scale real temporal networks to uncover reachability transitions in their global connectedness.

Many dynamical processes evolving on networks are related to the problem of reachability, determining the ability of a structure to maintain a global phenomenon. Reachability changes radically if one considers the time-varying nature of connections between network nodes [1], instead of deeming them static. Time induces an inherent direction of connectivity, as it restricts the direction of influence or information flow in the structure. This in turn has an impact on dynamical processes evolving on such networks, such as spreading [2–4], social contagion [5, 6] ad-hoc message passing by mobile agents [7] or routing dynamics [8]. In all these processes interacting entities may have limited memory thus can only use paths constrained by limited waiting times, further restricting the eligible temporal structure for their global emergence.

Directed percolation (DP) is a paradigmatic example to characterise connectivity in temporal systems. This process exhibits dynamical phase transitions into absorbing states with a well-defined set of universal critical exponents [9–12]. Originally introduced in 1957 [13] and further developed later [14], DP has attracted a considerable amount of work in the physics literature. It has applications in reaction-diffusion systems [15], star formation in galaxies [16], conduction in strong electric fields in semiconductors [17], and biological evolution [18]. While it is straightforward to define idealised models governed by DP, such as lattice models [19–25], its features are more difficult to realize in nature [12, 26], allowing only a few recent experimental realisations of DP [27, 28]. Nevertheless, this description is advantageous in providing an understanding of the connectivity of temporal structures to describe ongoing dynamical processes [29–39].

There is a thorough theoretical understanding of static network connectivity with several analytic and computational concepts borrowed from percolation theory. Concepts such as phase transitions, giant components, and susceptibility, which were developed formally for large lattices and random networks, are extremely useful and routinely used to analyse real-world networks and processes, for example, disease spreading [40–43]. Connec-

tivity is a central property of temporal networks too, with several recent techniques to characterise it, e.g. by using limited waiting time reachability [44–48]. However, previous works on the theory of temporal connectivity [39, 49, 50] fundamentally rely on different notions of connectivity of structure, such as static connectivity, deterministic walks, or networks consisting of discrete temporal layers. Here we take a step back from this position to study the problem of reachability in temporal networks as a directed percolation process, which is a natural choice to consider the inherent directionality induced by time in these constructs.

A temporal network $G = (\mathcal{V}, \mathcal{E}, \mathcal{T})$ is defined as a set of nodes \mathcal{V} connected through events $e = (\mathbf{u}, \mathbf{v}, t_{\text{start}}, t_{\text{end}}) \in \mathcal{E}$, each of which represents an interaction of two subsets of nodes $\mathbf{u}, \mathbf{v} \subseteq \mathcal{V}$ between times of $t_{\text{start}}, t_{\text{end}} \in \mathcal{T}$ ($t_{\text{start}} < t_{\text{end}}$) during an observation period \mathcal{T} . The connectivity of events is characterised by time-respecting paths [33, 51], defined as sequences of adjacent events $e \rightarrow e'$. Here we call two events $e, e' \in \mathcal{E}$ adjacent if they follow each other in time ($t'_{\text{start}} > t_{\text{end}}$) and share at least one ending node in common ($\mathbf{v} \cap \mathbf{u}' \neq \emptyset$) as schematically demonstrated in Fig. 1a. For simplicity, we assume that temporal network events are instantaneous ($t_{\text{start}} = t_{\text{end}}$) and represent undirected interactions between single nodes ($\mathbf{u} = \mathbf{v} = \{i, j\}$ where $i, j \in \mathcal{V}$ and $i \neq j$), if we do not mention otherwise. All of our notations can be easily extended for directed events with duration.

While time-respecting paths code the possible routes of information or influence spreading on a temporal network, some dynamical processes have further restrictions on the time during which they can propagate further after reaching a node. An example of such limited local lifetime processes is the spreading of a disease, where infected nodes may recover after some time, thus becoming unable to further infect any other node, unless re-infected. In our definition, we define limited waiting-times in temporal paths by allowing adjacent events to be connected if they are not separated temporally by more than a $t'_{\text{start}} - t_{\text{end}} < \delta t$ time window. This quantity con-

trols the connectivity of the temporal network. In contrast to the control parameters based on node or event occupation probabilities, which could be used to adjust the overall activity level of the network, changing δt modifies the behaviour of the spreading itself. A compact way of describing this problem is provided by weighted event graphs $D = (\mathcal{E}, E_D, \Delta t(e, e'))$, a higher-order static directed acyclic graph representation of temporal networks [50]. In this description events act as nodes and two events are connected through a directed, weighted link if they are adjacent, i.e. $E_D = \{(e, e') \mid e \rightarrow e'\}$ with weights defined as $\Delta t(e, e') = t'_{\text{start}} - t_{\text{end}}$, the time between the two adjacent events. The event graph contains a superposition of all temporal paths [52] and retains the arrow of time even after turning the temporal structure into a static, directed one (Fig. 1b). Superposition of all δt limited-time temporal paths can be achieved by constructing the event graph of a temporal network and removing all the event graph links with weights larger than δt (see Fig. 1c).

Furthermore, we define the reduced temporal event graph \hat{D} , where only the first adjacency relationships per node are preserved for each node in D . It has a maximum of two incoming and two outgoing links for each node yet it contains all the reachability relationships of the original temporal network [53]. That is, the reduced event graph exactly retains the reachability of the temporal network for a given value of δt by removing redundant adjacency relationships (feed-forward loops) between events. The reduction allows one to interpret the three possible out-degrees using the terminology of DP as annihilation (0), diffusion (1), and decoagulation (2) in the case the out-neighbours are not already reachable through some longer loop. This upper bound on in- and out-degrees after reduction is valid for any temporal network where the probability of adjacent events happening at exactly the same time is negligible. See Supplementary Materials (SM) for more details on the reduction of event graphs.

Order parameters and other characteristics. Compared to static structures, temporal networks incorporate time as an additional degree of freedom, which introduces an extra dimension to the characterisation of their structural phase-transition of connectivity around a critical point. This is similar to DP where dimensions are related to space and time with associated independent critical exponents [54, 55]. To observe connectivity, we measure the expected δt -limited waiting-time reachability of a spreading process starting from a random event. We are interested in the number of unique nodes $V \subseteq \mathcal{V}$, that are reachable from the source of spreading, the time duration of the longest path (i.e. its lifetime [50]) $T \subseteq \mathcal{T}$, and the total number of reachable events $M \subseteq \mathcal{E}$, in this component. These are analogous to mean spatial volume, mean survival time, and mean cluster mass in the DP formalism (respectively) [9, 12]. Further, in paral-

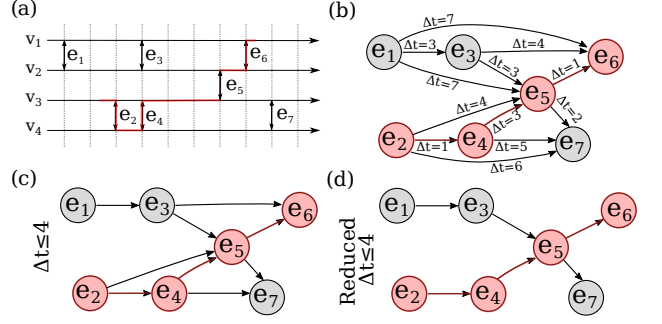


FIG. 1. Different representations of an instantaneous, undirected temporal network. (a) Vertices v_i are connected via dyadic instantaneous events e_j . (b) Weighted temporal event graph is a directed acyclic graph where adjacent events are connected via links directed by time. Link weights are defined as the time difference Δt between connected events. Paths in an event graph are equivalent to time-respecting paths [52]. (c) Waiting-time constrained event graphs with links of weights $\Delta t \leq \delta t$ removed contain all δt -limited paths. (d) Reduced event graph in which locally redundant links are removed (see main text). The highlighted line represents a time respecting path (a) and its equivalent path over event graph (b,c) and reduced event graph (d).

lel to DP, we define the survival probability $P(t)$ as the probability that there is a path from a randomly selected initial source event to an event after time t . The ultimate survival probability $P_\infty = \lim_{t \rightarrow \infty} P(t)$ is then the survival probability at large values of t . Note, that when we defined these quantities we have opted for simplicity (see SM for discussion) but one could define them in slightly different ways depending on the physical question.

Using the maximum waiting time δt as a control parameter is a natural choice as it has a clear physical interpretation. However, it is a quantity, which scale depends on the timescales of the system, unlike occupation probabilities that are typically used as control parameters in DP. Further, although it is related to the local connectivity, this relationship is indirect and might depend e.g. on the temporal inhomogeneities in interaction sequences. For this reason, we define another control parameter that directly measures the local connectivity of the system. We use the local effective connectivity $\hat{q}^{\text{out}}(\delta t)$, which is the average excess out-degree of the reduced event graph $\hat{D}(\delta t)$. This is a monotonically increasing function of δt , which normalizes the changes in connectivity given by the changes in the maximum allowed waiting time δt . We then centralise this quantity by subtracting its value from its phase-transition critical point \hat{q}_c^{out} , and denote the resulting control parameter as $\tau = \hat{q}^{\text{out}} - \hat{q}_c^{\text{out}}$.

In addition to the single-source scenario where we assume the component to start from a single node in D , we investigate a fully occupied homogeneous initial condition, where we compute paths starting from all nodes at an initial time t_0 . Analogous to DP, we define par-

ticle density $\rho(t)$ as the fraction of infected nodes in D at time t , while stationary density $\rho_{\text{stat}}(\tau)$, the order parameter, is defined as the particle density after the system reached a stationary state. We can also add the effects of an external field h to this scenario. In continuous-time, this would be equivalent to the spontaneous emergence of sources of infection, and thus occupation of nodes in D (events in G) through an independent Poisson point process with a rate of h . Susceptibility $\chi(\tau, h) = \frac{\partial}{\partial h} \rho_{\text{stat}}(\tau, h)$ can then be measured by the rate of change in stationary density as the external field changes [12]. Note that unlike percolation in static networks, where it is possible to estimate susceptibility e.g. by computing the second moment of the cluster size distribution, such methods are not directly applicable here.

Critical behavior in random systems. Next, we derive a mean-field approximation for the above defined measures and identify the critical point. For simplicity, we focus on temporal networks based on an underlying static structure, where events are induced via links activated by independent and identical continuous-time stochastic processes. In the reduced event graph \hat{D} of this induced temporal network G , we can write the probability of observing a node (i.e., an event in G) with a given out-degree. Given the excess degrees l and r of the two temporal network nodes in G incident to the link corresponding to the event $e \in \mathcal{E}$, we can compute the probability of a zero out-degree for a node in \hat{D} as $\hat{p}_0^{\text{out}} = \Pi_{\delta t} \hat{\Pi}_{\delta t}^{l+r}$. Here $\Pi_{\delta t}$ is the cumulative inter-event time distribution induced by a link activation process for a given δt , and $\hat{\Pi}_{\delta t}$ is the corresponding cumulative residual waiting time distribution. Similarly, for out-degree 2, we can compute $\hat{p}_2^{\text{out}} = \int_0^\infty (1 - \hat{\Pi}_{\min \delta t, t}^l)(1 - \hat{\Pi}_{\min \delta t, t}^r) \pi_t dt$, where π_t is the inter-event time distribution. Given that the maximum out-degree of events in the reduced event graph is 2, the \hat{p}_1^{out} can be derived as $\hat{p}_1^{\text{out}} = 1 - \hat{p}_0^{\text{out}} - \hat{p}_2^{\text{out}}$. Note that these probabilities can be similarly derived for in-degrees by reversing the direction of time.

The joint in- and out-degree distribution of the event graph can be computed from the excess degree distribution q_k of the underlying static network. If the degrees are independent, this becomes $\hat{p}_{i,o}^{\text{in,out}} = \sum_{l,r} \hat{p}_i^{\text{in}} \hat{p}_o^{\text{out}} q_l q_r$. We will denote the generating function of the joint degree distribution as $\mathcal{G}_0(z_{\text{in}}, z_{\text{out}})$ and the corresponding out excess degree distribution as $\mathcal{G}_1^{\text{out}}(z_{\text{out}})$. We construct the mean-field rate equation for occupation density $\rho(t)$ in homogeneous occupation initial condition using the excess out-degree distribution of the event graph $\hat{q}_k^{\text{out}} = \frac{d^k}{k! dz^k} G_1^{\text{out}}(z)|_{z=0}$. The excess out-degree of nodes in the event graph \hat{D} gives the change in the number of further nodes we can reach from an already reached node: nodes with out-degree 2 increase the number of reached nodes by one, nodes with out-degree 1 do not have any effect on the number of reached nodes, and out-degree

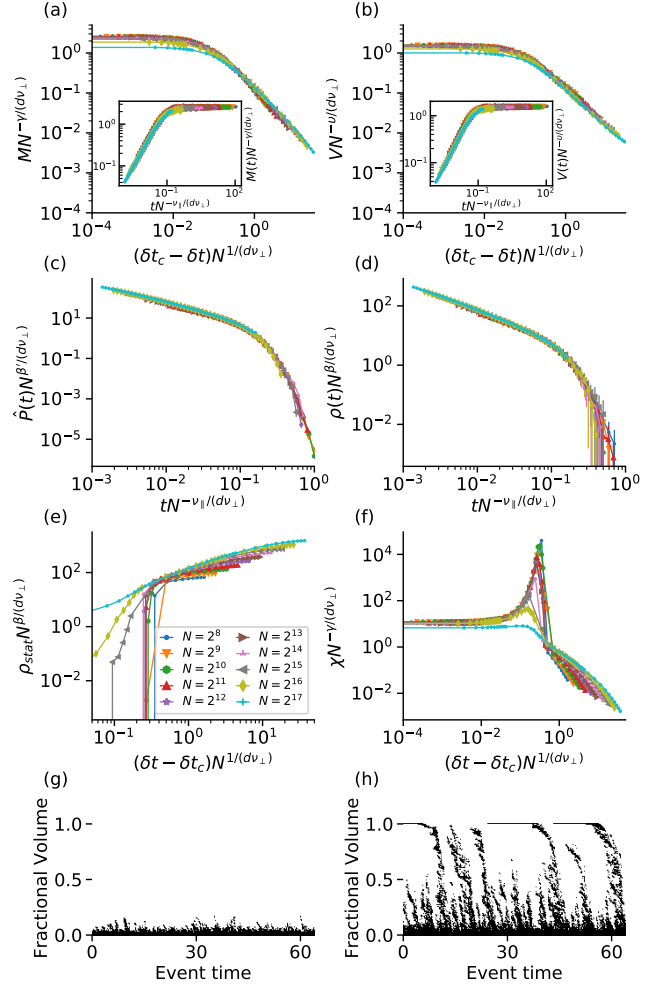


FIG. 2. (a) Mean cluster mass M , (b) volume V and (c) survival probability $\hat{P}(t)$ for single source spreading scenarios, after finite-size scaling. (a inset) Mean cluster mass and (b inset) volume from a single source as a function of time from beginning of the spreading process after finite-size scaling. (d) Particle density $\rho(t)$, (e) static density ρ_{stat} and (f) susceptibility $\chi(\delta t, 0)$ as a function of δt for the homogeneous initial condition. Measurements are averaged over at least 256 (up to 4096) realisations of temporal network constructed from random 9-regular networks ($N \in \{2^8, 2^9, \dots, 2^{17}\}$) and Poisson point process activations $\lambda = 1$ of links. All functions of time (a and b insets and panels c and d) are measured at $\delta t = \delta t_c = 0.08808$. d is set to DP upper critical dimension $d_c = 4$. Observing temporal connectivity profiles (i.e., relative cluster volumes for each event, see main text) for a single realisation of 9-regular network with Poisson process ($N = 1024$, $\lambda = 1$, $0 < t < 64$) for before ($\delta t = 0.07$, panel g) and after the critical $\delta t = 0.092$ (panel h) shows that for $\delta t > \delta t_c$ components grow to a size comparable the network.

0 nodes reduces by one the number of reached nodes. That is, the total change is $\hat{q}_2^{\text{out}} - \hat{q}_0^{\text{out}}$. In addition, some nodes we can reach are already reachable through some other paths. In total we reach on expectation $\hat{q}_1^{\text{out}} + 2\hat{q}_2^{\text{out}}$ nodes and each of them have probability of $\rho(t)$ of being

already reached. The rate equation becomes

$$\partial_t \rho(t) = [\hat{q}_2^{\text{out}} - \hat{q}_0^{\text{out}}] \rho(t) - [\hat{q}_1^{\text{out}} + 2\hat{q}_2^{\text{out}}] \rho^2(t). \quad (1)$$

In this equation the values of \hat{q}_k^{out} are constants in time. Noting the critical point for this equation as $\hat{q}_2^{\text{out}} - \hat{q}_0^{\text{out}} = 0$, and that the expected value is by definition $\hat{q}^{\text{out}} = \hat{q}_1^{\text{out}} + 2\hat{q}_2^{\text{out}}$, and that $\hat{q}_2^{\text{out}} - \hat{q}_0^{\text{out}} = \hat{q}^{\text{out}} - 1$, we can write Eq. (1) as $\partial_t \rho(t) = \tau \rho(t) - \hat{q}^{\text{out}} \rho^2(t)$.

The Eq. (1) follows the same form as the DP mean-field equation for a $d + 1$ -dimensional lattice [12] and it can be solved explicitly (see SM). It has the critical point at $\tau = 0$, while it indicates that $\rho \rightarrow \tau/\hat{q}^{\text{out}}$ for $\tau > 0$. Asymptotically it provides the critical exponents as

$$\begin{aligned} \rho(t) &\sim t^{-\alpha}, & \text{if } \tau = 0 \\ \rho_{\text{stat}}(\tau) &\sim \tau^\beta, & \text{if } \tau > 0 \text{ and } t \rightarrow \infty \end{aligned} \quad (2)$$

with values $\alpha = \beta = 1$, where $\alpha = \beta/\nu_{\parallel}$ and ν_{\parallel} is the temporal correlation length exponent, in accordance with the corresponding mean-field DP critical exponents [12].

The expected out-component size, i.e. the mean cluster mass M , can be computed from the joint degree distribution of the event graph \hat{D} by assuming that it is a random directed graph with the same joint in- and out-degree distribution as \hat{D} . The out-component size distribution can be derived from $H_0(z_{\text{out}}) = z_{\text{out}} \mathcal{G}_0(1, H_1(z_{\text{out}}))$, $H_1(z_{\text{out}}) = z_{\text{out}} \mathcal{G}_1^{\text{out}}(H_1(z_{\text{out}}))$, and the mean out-component size can be written as $M = \frac{\partial H_0(z_{\text{out}})}{\partial z_{\text{out}}} \big|_{z_{\text{out}}=1}$ [56]. These equations, when $\tau \rightarrow 0^-$, lead to $M \sim -\tau^{-\gamma}$ with $\gamma = 1$ (see SM). Here $\gamma = \nu_{\parallel} + d\nu_{\perp} - \beta - \beta'$, matching the mean-field exponent of mean cluster mass in DP [12]. Here ν_{\perp} indicates the spatial temporal correlation exponent.

The survival probability of a component, $P(t)$, is measured by the out-component sizes of nodes in the event graph and the occupation density, $\rho(t)$, is calculated by the in-component sizes of all possibly reachable nodes, which means that these two quantities are equal $\rho(t) = P(t)$ (see SM). Consequently, given the control parameter τ , $\rho_{\text{stat}}(\tau) = P_{\infty}(\tau)$ as long as the time-reversed event graph has the same probability of being generated as the original one (e.g. if $\forall_{i,o} p_{i,o}^{\text{in,out}} = p_{o,i}^{\text{in,out}}$). This leads us to the rapidity-reversal symmetry for event graphs similarly characterizing DP [57] where $\beta = \beta'$ and $P_{\infty}(\tau) \sim \tau^{\beta'}$.

Finite-size scaling in random systems. The previous mean-field solutions were obtained by approximating the event graph of a random temporal network with a random directed graph with the same joint in- and out-degree distribution. Alternatively, the same critical exponents can be empirically verified by using finite-size scaling of the system close to its percolation critical point, where its large-scale properties become invariant under scale transformations. To do so we simulate random temporal networks of varying size and perform computationally efficient reachability estimations [45] from single-seed and homogeneous fully occupied initial conditions to

compute the macroscopic scaling quantities. We expect that data points would collapse when using the correct critical exponents of β , ν_{\parallel} and ν_{\perp} corresponding to the mean-field values approximated for directed percolation. Note since there is no metric in space, so ν_{\perp} is simply defined using the characteristic volume of the cluster, V .

Our finite-size scaling analysis confirms the validity of all these DP mean-field exponents to characterise the percolation phase transition of random temporal networks. This is demonstrated in Fig. 2a-f for temporal networks induced on a 9-regular network with links activated via independent Poisson processes. These results are robust in the presence of several types of temporal and spatial heterogeneities, as similar data collapse can be seen in a multitude of combinations of static network topologies (including one- to four-dimensional square lattices and random d -regular networks in addition to Erdős-Rényi random networks) and temporal dynamics (including bursty heavy-tail inter-event time processes and self-exciting dynamics in addition to Poisson dynamics) as we demonstrate in Ref. [58].

DP measures in real-world temporal networks. To quantify the time scales related to the reachability transitions in real settings, we measure the same macroscopic quantities as before for single source and homogeneous initial conditions for four different real-world systems (Fig. 3a-d). We concentrate on temporal networks describing an air transportation system (Fig. 3a), the public transportation of Helsinki (Fig. 3b), a large Twitter mention network (Fig. 3c), and a mobile phone call network of millions of individuals (Fig. 3d). For details on the data sets and pre-processing, see SM. In each system, there is clear evidence of an absorbing to active phase transition in terms of M , V , and ρ_{stat} . Note that even though these quantities describe the same transition process as a function of the control parameter, their scales are not directly comparable. In some systems, some of these quantities can be re-scaled in a way that they follow each other (for example, V and M in the transportation network shown in Fig. 3b), but in general the curves representing the various ways of measuring component sizes behave in different ways after the phase transition. This highlights the fact that distinguishing between the different notions of connectivity in temporal networks can be important in practical terms. Further, contrary to the simple theoretical models, we see multiple peaks in the susceptibility curves of the public transport and Twitter networks, which indicates the existence of multiple time scales relative to the connectivity of the data.

The reachability phase transition behaviour can be better understood by investigating temporal connectivity profiles represented by cluster volumes. This is measured as the time evolution of the number of unique temporal network nodes in the out-component of a spreading process starting initiated from each event. For random networks below the critical point (see Fig. 2g) only small

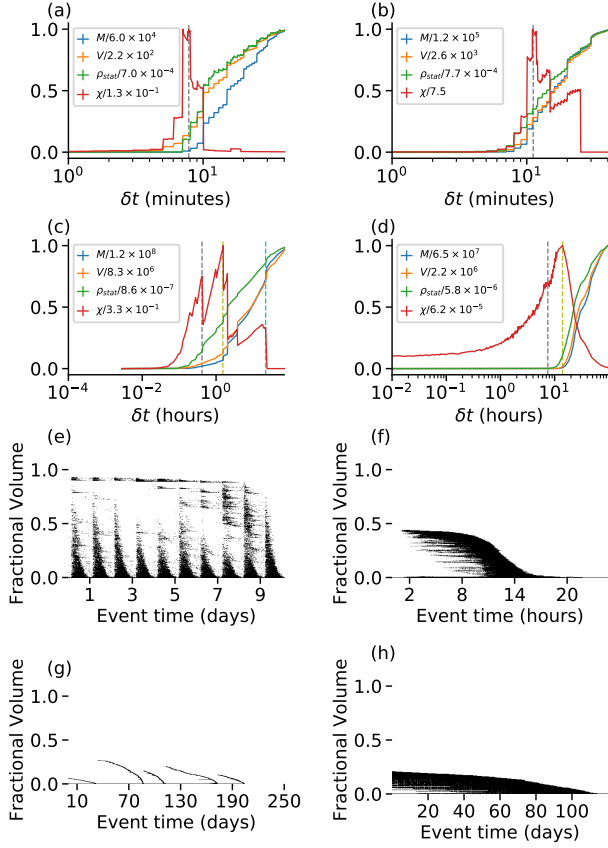


FIG. 3. Mean cluster mass M , mean cluster volume V , static density ρ_{stat} and susceptibility $\chi(\delta t, 0)$ as a function of δt for four real-world networks: (a) Air transport [59], (b) Helsinki public transportation [60], (c) Twitter mentions [61] and (d) mobile phone calls [62] display an absorbing to active phase transition around 470 seconds, 670 seconds, 25 minutes and 7.5 hours respectively, as indicated by change from very small values for M , V and ρ_{stat} to values comparable to the size of the system and a peak in susceptibility $\chi(\delta t, 0)$. Mobile and Twitter networks show a second peak in susceptibility around 1.5 hours and 22 hours respectively and twitter data shows a third peak around 14 hours. The temporal reachability profiles display relative cluster volumes for each event as a function of the event time. They are shown close to δt_c for (e) air transport, (f) Helsinki public transportation, (g) Twitter mentions and (h) mobile phone call networks.

components appear. However, around the critical point (Fig. 2h), multiple large components evolve representing structures where spreading from some events can reach a significant fraction of nodes although these components do not overlap in time as they span only a short period of the whole timeline. A similar column structure can be observed for the air transport network and the Twitter network (Fig. 3e,g) too. However, in the air transportation network, the column structure is regular, following the daily pattern of flights. In the Twitter network, the components never reach all the nodes in the temporal

network due to the larger separation of temporal components, and their structure reflects the rare emergence of possible macroscopic cascades in this system. The public transport network (spanning a single day) and the mobile phone network display a single wing-like structure (Fig. 3f,h). This structure is induced by early components that can reach a significant fraction of the network, which are then joined by other components reaching smaller subsets of nodes. This is also indicated by the long horizontal line structures under the wings. The temporal reachability profiles provide a useful tool for understanding how the connectivity transition takes place at the system level, and they serve as a starting point for a more detailed analysis of the individual systems and their inhomogeneities.

Conclusion. Connectivity of complex networks is one of their most important global property as it codes the possible routes of information and in turn determines disease spreading, transportation routes, and information diffusion in real settings. This is a major challenge as time-varying interactions induce time-dependent connectivity and can have dramatic effects on the speed and volume of any ongoing dynamical process [2–4]. A concise theory of temporal connectedness is a necessary step forward from the limited description that static networks provide. Our results map the temporal network connectivity problem to directed percolation, this way opening the door for detailed and well-established descriptions of the critical phase transitions characterising limited waiting-time processes on temporal networks. Further, our framework provides a crucial tool for characterising and more precise modelling of spreading and diffusion phenomena, even in real-world settings.

Acknowledgement. We would like to thank János Kertész and Géza Ódor for their helpful comments and suggestions. The authors wish to acknowledge CSC – IT Center for Science, Finland, and Aalto University “Science-IT” project for generous computational resources. Márton Karsai acknowledges support from the DataRedux ANR project (ANR-19-CE46-0008) and the SoBigData++ H2020 project (H2020-871042).

-
- [1] P. Holme and J. Saramäki, *Temporal Network Theory*, Computational Social Sciences (Springer International Publishing, 2019).
 - [2] R. Lambiotte and N. Masuda, *A guide to temporal networks*, Vol. 4 (World Scientific, 2016).
 - [3] P. Holme and J. Saramäki, Temporal networks, *Physics reports* **519**, 97 (2012).
 - [4] P. Holme, Modern temporal network theory: a colloquium, *The European Physical Journal B* **88**, 234 (2015).
 - [5] D. J. Daley and D. G. Kendall, Epidemics and rumours, *Nature* **204**, 1118 (1964).
 - [6] C. Castellano, S. Fortunato, and V. Loreto, Statistical physics of social dynamics, *Reviews of modern physics*

- 81**, 591 (2009).
- [7] C. Tripp-Barba, C. Alcaraz, and M. A. Igartua, Special issue on “modeling and performance evaluation of wireless ad-hoc networks”, *Ad Hoc Networks* **52**, 1 (2016).
 - [8] N. Nassir, M. Hickman, A. Malekzadeh, and E. Irannezhad, A utility-based travel impedance measure for public transit network accessibility, *Transportation Research Part A: Policy and Practice* **88**, 26 (2016).
 - [9] H. Hinrichsen, Non-equilibrium critical phenomena and phase transitions into absorbing states, *Advances in physics* **49**, 815 (2000).
 - [10] G. Ódor, Universality classes in nonequilibrium lattice systems, *Reviews of modern physics* **76**, 663 (2004).
 - [11] H. Hinrichsen, Non-equilibrium phase transitions, *Physica A: Statistical Mechanics and its Applications* **369**, 1 (2006).
 - [12] M. Henkel, H. Hinrichsen, S. Lübeck, and M. Pleimling, *Non-equilibrium phase transitions*, Vol. 1 (Springer, 2008).
 - [13] S. R. Broadbent and J. M. Hammersley, Percolation processes: I. crystals and mazes, in *Mathematical Proceedings of the Cambridge Philosophical Society*, Vol. 53 (Cambridge University Press, 1957) pp. 629–641.
 - [14] J. Blease, Directed-bond percolation on hypercubic lattices, *Journal of Physics C: Solid State Physics* **10**, 925 (1977).
 - [15] F. Schlögl, Chemical reaction models for non-equilibrium phase transitions, *Zeitschrift für physik* **253**, 147 (1972).
 - [16] H. Gerola, P. Seiden, and L. Schulman, Theory of dwarf galaxies, *The Astrophysical Journal* **242**, 517 (1980).
 - [17] N. Van Lien and B. Shklovskii, Hopping conduction in strong electric fields and directed percolation, *Solid State Communications* **38**, 99 (1981).
 - [18] P. Bak and K. Sneppen, Punctuated equilibrium and criticality in a simple model of evolution, *Physical review letters* **71**, 4083 (1993).
 - [19] E. Domany and W. Kinzel, Equivalence of cellular automata to ising models and directed percolation, *Physical review letters* **53**, 311 (1984).
 - [20] W. Kinzel, Phase transitions of cellular automata, *Zeitschrift für Physik B Condensed Matter* **58**, 229 (1985).
 - [21] T. E. Harris, Contact interactions on a lattice, *The Annals of Probability* , 969 (1974).
 - [22] I. Jensen, Critical behavior of the pair contact process, *Physical review letters* **70**, 1465 (1993).
 - [23] J. Mendes, R. Dickman, M. Henkel, and M. C. Marques, Generalized scaling for models with multiple absorbing states, *Journal of Physics A: Mathematical and General* **27**, 3019 (1994).
 - [24] R. M. Ziff, E. Gulari, and Y. Barshad, Kinetic phase transitions in an irreversible surface-reaction model, *Physical review letters* **56**, 2553 (1986).
 - [25] D. Dhar, The collapse of directed animals, *Journal of Physics A: Mathematical and General* **20**, L847 (1987).
 - [26] H. Hinrichsen, On possible experimental realizations of directed percolation, *Brazilian Journal of Physics* **30**, 69 (2000).
 - [27] K. A. Takeuchi, M. Kuroda, H. Chaté, and M. Sano, Directed percolation criticality in turbulent liquid crystals, *Physical review letters* **99**, 234503 (2007).
 - [28] G. Lemoult, L. Shi, K. Avila, S. V. Jalikop, M. Avila, and B. Hof, Directed percolation phase transition to sustained turbulence in couette flow, *Nature Physics* **12**, 254 (2016).
 - [29] A. Barrat, M. Barthélemy, and A. Vespignani, *Dynamical processes on complex networks* (Cambridge university press, 2008).
 - [30] R. Pastor-Satorras, C. Castellano, P. Van Mieghem, and A. Vespignani, Epidemic processes in complex networks, *Reviews of modern physics* **87**, 925 (2015).
 - [31] D. Kempe, J. Kleinberg, and A. Kumar, Connectivity and inference problems for temporal networks, *Journal of Computer and System Sciences* **64**, 820 (2002).
 - [32] J. Moody, The importance of relationship timing for diffusion, *Social forces* **81**, 25 (2002).
 - [33] P. Holme, Network reachability of real-world contact sequences, *Physical Review E* **71**, 046119 (2005).
 - [34] R. K. Pan and J. Saramäki, Path lengths, correlations, and centrality in temporal networks, *Physical Review E* **84**, 016105 (2011).
 - [35] I. Scholtes, N. Wider, R. Pfitzner, A. Garas, C. J. Tesse, and F. Schweitzer, Causality-driven slow-down and speed-up of diffusion in non-markovian temporal networks, *Nature communications* **5**, 1 (2014).
 - [36] J. Stehlé, N. Voirin, A. Barrat, C. Cattuto, L. Isella, J.-F. Pinton, M. Quaggiotto, W. Van den Broeck, C. Régis, B. Lina, *et al.*, High-resolution measurements of face-to-face contact patterns in a primary school, *PloS one* **6**, e23176 (2011).
 - [37] S. Dai, H. Bouchet, A. Nardy, E. Fleury, J.-P. Chevrot, and M. Karsai, Temporal social network reconstruction using wireless proximity sensors: model selection and consequences, *EPJ Data Science* **9**, 19 (2020).
 - [38] A. Aleta, G. F. de Arruda, and Y. Moreno, Data-driven contact structures: from homogeneous mixing to multilayer networks, *PLOS Computational Biology* **16**, 1 (2020).
 - [39] R. Parshani, M. Dickison, R. Cohen, H. E. Stanley, and S. Havlin, Dynamic networks and directed percolation, *EPL (Europhysics Letters)* **90**, 38004 (2010).
 - [40] M. E. Newman, Spread of epidemic disease on networks, *Physical review E* **66**, 016128 (2002).
 - [41] E. Kenah and J. M. Robins, Second look at the spread of epidemics on networks, *Physical Review E* **76**, 036113 (2007).
 - [42] E. Kenah and J. C. Miller, Epidemic percolation networks, epidemic outcomes, and interventions, *Interdisciplinary perspectives on infectious diseases* **2011**, 10.1155/2011/543520 (2011).
 - [43] A. K. Rizi, A. Faeqeh, A. Badie-Modiri, and M. Kivelä, Epidemic spreading and digital contact tracing: Effects of heterogeneous mixing and quarantine failures, *arXiv:2103.12634* (2021).
 - [44] P. Crescenzi, C. Magnien, and A. Marino, Approximating the temporal neighbourhood function of large temporal graphs, *Algorithms* **12**, 211 (2019).
 - [45] A. Badie-Modiri, M. Karsai, and M. Kivelä, Efficient limited-time reachability estimation in temporal networks, *Phys. Rev. E* **101**, 052303 (2020).
 - [46] A. Casteigts, A.-S. Himmel, H. Molter, and P. Zschoche, The computational complexity of finding temporal paths under waiting time constraints, *arXiv:1909.06437* (2019).
 - [47] S. Thejaswi, J. Lauri, and A. Gionis, Restless reachability problems in temporal graphs, *arXiv:2010.08423* <https://arxiv.org/abs/2010.08423> (2020).

- [48] A.-S. Himmel, M. Bentert, A. Nichterlein, and R. Niedermeier, Efficient computation of optimal temporal walks under waiting-time constraints, in *International Conference on Complex Networks and Their Applications* (Springer, 2019) pp. 494–506.
- [49] M. Starnini and R. Pastor-Satorras, Temporal percolation in activity-driven networks, *Physical Review E* **89**, 032807 (2014).
- [50] M. Kivelä, J. Cambe, J. Saramäki, and M. Karsai, Mapping temporal-network percolation to weighted, static event graphs, *Scientific reports* **8**, 1 (2018).
- [51] H. H. Lentz, T. Selhorst, and I. M. Sokolov, Unfolding accessibility provides a macroscopic approach to temporal networks, *Physical review letters* **110**, 118701 (2013).
- [52] J. Saramäki, M. Kivelä, and M. Karsai, Weighted temporal event graphs, in *Temporal Network Theory* (Springer, 2019) pp. 107–128.
- [53] A. Mellor, The temporal event graph, *Journal of Complex Networks* **6**, 639 (2017).
- [54] P. Grassberger, On phase transitions in Schögl’s second model, *Zeitschrift für Physik B Condensed Matter* **47**, 365 (1982).
- [55] H. K. Janssen, On the nonequilibrium phase transition in reaction-diffusion systems with an absorbing stationary state, *Zeitschrift für Physik B Condensed Matter* **42**, 151 (1981).
- [56] M. E. Newman, S. H. Strogatz, and D. J. Watts, Random graphs with arbitrary degree distributions and their applications, *Physical review E* **64**, 026118 (2001).
- [57] P. Grassberger and A. De La Torre, Reggeon field theory (schögl’s first model) on a lattice: Monte carlo calculations of critical behaviour, *Annals of Physics* **122**, 373 (1979).
- [58] A. Badie-Modiri, A. K. Rizi, M. Karsai, and M. Kiveä, Directed percolation in random temporal network models with heterogeneities (2021), (in preparation).
- [59] Bureau of Transportation Statistics, (2017).
- [60] R. Kujala, C. Weckström, R. K. Darst, M. N. Mladenović, and J. Saramäki, A collection of public transport network data sets for 25 cities, *Scientific data* **5**, 180089 (2018).
- [61] J. Yang and J. Leskovec, Patterns of temporal variation in online media, in *Proceedings of the fourth ACM international conference on Web search and data mining* (ACM, 2011) pp. 177–186.
- [62] M. Karsai, M. Kivelä, R. K. Pan, K. Kaski, J. Kertész, A.-L. Barabási, and J. Saramäki, Small but slow world: How network topology and burstiness slow down spreading, *Physical Review E* **83**, 025102(R) (2011).

Supplementary Material for Directed Percolation in Temporal Networks

Arash Badie-Modiri,¹ Abbas K. Rizi,¹ Márton Karsai,^{2,3} and Mikko Kivelä¹

¹Department of Computer Science, School of Science, Aalto University, FI-0007, Finland

²Department of Network and Data Science Central European University, 1100 Vienna, Austria

³Alfréd Rényi Institute of Mathematics, 1053 Budapest, Hungary

(Dated: April 6, 2024)

GENERATING SYNTHETIC TEMPORAL NETWORKS AND THE EVENT GRAPH

The synthetic temporal networks are created with some continuous-time stochastic process based on an underlying static network with a degree distribution of p_k and excess degree distribution of q_k . The event graph, directed acyclic graph of adjacency relationships between pairs events, can then be produced by iterating through all events e and connecting it to all other events when e happens less than δt time before that event and they share at least one node.

Reachability on the event graph will be preserved by removing some of the links so that the in/out-degree varies between 0 to 2 for every node [1] as long as the probability of adjacent events happening at exactly the same time is negligible. Practically, for every event e in the event graph, we can remove directed links to all but the very first events for each of the two nodes involved in e . This preserves connectivity in the event graph since all the events on the other end of the removed adjacency relationships would still be connected through one of the remaining links out-bound from e as they share at least one node and the time difference is less than or equal to the original event. Note that if more than one adjacent events are happening at the same time and no other adjacent events happen before them, we would have to keep all of them to preserve connectivity.

Note that in practice it is often not necessary to explicitly generate the event graph to measure the quantities. It is possible to store the list of associated events for each node in the network sorted by time and generate adjacency relationships on the fly. This can also be combined with other techniques such as using probabilistic data structures for estimating out-component sizes to allow processing of temporal networks much larger than what is possible with the explicit solution [2].

Degree distribution of the reduced event graph

Let's assume a vertex on the event graph, an event e , that involves two nodes called l and r which just activated at time t_0 (Fig 1). The two nodes l and r have respectively q_l and q_r neighbor nodes, other than each other, over the static network.

Let's also define $Pr(t_{res} < \delta t)$ as the probability that a

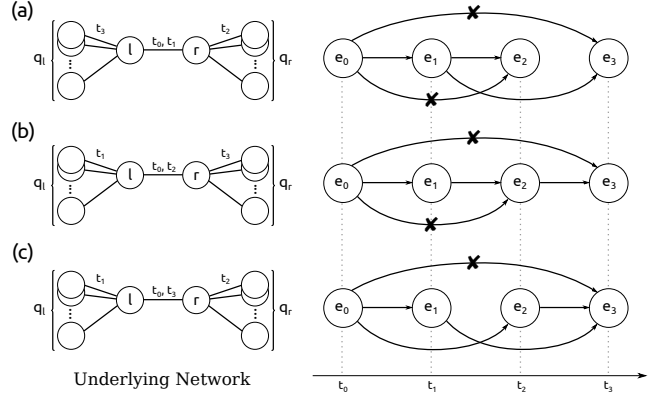


FIG. 1. Considering the case of an event between nodes l and r happening at time t_0 , where each node has q_l and q_r neighbours other than each other respectively. Assuming link $l-r$ was selected uniformly at random from the set of all the links in the base network, the values q_l and q_r are both realisations of the excess degree distribution of the base network P_q . Out-degree of the event $e_0 = (l, r, t_0)$ is between zero and two depending on the order and timing of events between l , r and their neighbours. If the $l-r$ link activates before any of the other links incident to l and r (panel a) or only links incident to l (or only r) other than $l-r$ fire before $l-r$ (panel b) at a time $t_1 > t_0$, event e_0 would have an out degree of zero if $t_1 - t_0 \geq \delta t$ or one if $t_1 - t_0 < \delta t$. All other edges coming out of e_0 would necessarily get pruned out as shown by the crossed-out links. The only case for e_0 having a degree two happens when at least one event at $t_1 < \delta t$ only involving l and not r and one at $t_2 < \delta t$ only involving r and not l both happen before $l-r$ fires again.

process with inter-event time distribution \mathcal{T} can activate at least once in time δt after a random point in time. This can correspond to probability of one of the links in the underlying network activating within a time period of δt . Random variable t_{res} is distributed according to the residual inter-event time distribution \mathcal{R} . Similarly, $Pr(t_{iet} < \delta t)$ is the probability that a process with inter-event time distribution \mathcal{T} can activate at least once in time δt right after activation.

Probability of an event having out-degree of zero in the event graph can be calculated as:

$$P_{out}(0|q_l, q_r) = Pr(t_{res} > \delta t)^{q_l+q_r} Pr(t_{iet} > \delta t) \quad (1)$$

where q_l and q_r are the number of neighbours each of the nodes participating in the event has except for the connection between two nodes of the event in question, t_{iet}

is a realisation of the inter-event time distribution of the network \mathcal{T} and t_{res} is a realisation of the residual inter-event time distribution \mathcal{R} . Out-degree of an event is zero if and only if none of the $q_l + q_r$ adjacent links on the underlying network have an event within δt and the two nodes participating in the original event also don't have any events between them within δt . The second term corresponds to the probability of the same link not activating and the first is the probability of all of the other incident links except for the original link not activating in δt .

The only case that an event on the event graph can have an out-degree equal to 2 (as shown on Fig. 1c) is that at least one of the q_l neighbours of l and one of the q_r neighbours of r activate before δt and before reactivation of the link between l and r . Activation of the link between l and r before at least one of the links on each side is activated (Fig. 1a and 1b) would result in out-degree equal to zero or one depending on the value of δt and timing of the events.

Probability of having an out-degree equal to 2 can be calculated this way:

$$P_{out}(2|q_l, q_r) = \int_0^\infty (1 - Pr(t_{res} > \delta t \vee t_{res} > t)^{q_l}) (1 - Pr(t_{res} > \delta t \vee t_{res} > t)^{q_r}) Pr(t \sim \mathcal{T}) dt \quad (2)$$

where t_{res} , \mathcal{T} , q_l and q_r are defined as above. An event has an out-degree equal to 2 if and only if two mutually non-adjacent links adjacent to the link corresponding to the original event activated within δt and before the link corresponding to the original event is activated.

$$P_{out}(1|q_l, q_r) = 1 - (P_{out}(0|q_l, q_r) + P_{out}(2|q_l, q_r)) \quad (3)$$

Based on these equations, it is trivial to construct joint in- and out-degree distribution

$$P(in, out) = \sum_{q_l, q_r=1}^\infty P_{in}(in|q_l, q_r) P_{out}(out|q_l, q_r) P_q(q_l) P_q(q_r) \quad (4)$$

where $P_q(i)$ is the probability mass function of excess degree for the static aggregate base network.

It is possible to construct the joint degree distribution generating function \mathcal{G} using the joint degree distribution itself

$$\mathcal{G}(x, y) = \sum_{in, out=0}^2 P(in, out) x^{in} y^{out} \quad (5)$$

and in- and out-degree and excess degree distribution

generating functions

$$\begin{aligned} \mathcal{G}_0^{in}(x) &= \mathcal{G}(x, 1) \\ \mathcal{G}_0^{out}(y) &= \mathcal{G}(1, y) \\ \mathcal{G}_1^{in}(x) &= \frac{1}{z} \frac{\partial \mathcal{G}(x, y)}{\partial y} \Big|_{y=1} \\ \mathcal{G}_1^{out}(y) &= \frac{1}{z} \frac{\partial \mathcal{G}(x, y)}{\partial x} \Big|_{x=1} \end{aligned} \quad (6)$$

where z is the mean in- and out-degree derived from

$$z = \frac{\partial \mathcal{G}(x, y)}{\partial x} \Big|_{x=y=1} = \frac{\partial \mathcal{G}(x, y)}{\partial y} \Big|_{x=y=1}. \quad (7)$$

Note that the in- and out-excess degree distribution generating functions we just derived ($\mathcal{G}_1^{in}(x)$ and $\mathcal{G}_1^{out}(x)$) refer to excess in- and out-degree distribution of a random event in the event graph.

DETAILS OF ANALYTICAL DERIVATION OF CRITICAL EXPONENTS

To study properties of the event graph, we approximate it by a random directed graph with the same in- and out-degree distribution. The following sections are all based on this assumption. The validity of this assumption and the following results can be verified explicitly by empirically constructing temporal networks of different topologies and temporal dynamics and measuring scaling of quantities such as $\rho(t)$, $P(t)$, M , V or $\rho_{stat}(\tau)$ [3].

Control Parameter τ

The mean-field rate equation for occupation density in homogeneous occupation initial condition can be constructed as

$$\partial_t \rho(t) = [Q_{out}(2) - Q_{out}(0)]\rho(t) - [Q_{out}(1) + 2Q_{out}(2)]\rho^2(t) \quad (8)$$

where $Q_{out}(i) = \frac{\partial^i}{i! \partial y^i} \mathcal{G}_1^{out}(y)$ is the excess out-degree distribution of events in the event graph. Using excess degree distribution captures the fact that in the random temporal model we are using, in- and out-degrees of events in the event graph are correlated and both are a function of degree of the event's constituting nodes in the static base network. By defining $\tau = Q_{out}(2) - Q_{out}(0)$ and $g = Q_{out}(1) + 2Q_{out}(2)$, Eq. 8 turns into $\partial_t \rho(t) = \tau \rho(t) - g \rho^2(t)$ with stationary solutions at $\rho = 0$, which represents the absorbing phase, and $\tau = 0$, which corresponds to the mean-field critical point.

An event graph can be presented, without any change in reachability of any event, so that no event has an in- or out-degree larger than two (as discussed in the beginning

of this section) τ and g can be written as $\tau = \langle Q_{out} \rangle - 1$ and $g = \langle Q_{out} \rangle$.

The phase transition at $\tau = 0$ also complies with the previously known result of phase transition in random directed graphs with arbitrary degree distribution at $\frac{\partial}{\partial y} G_1^{out}(y)|_{y=1} = 1$ [4].

Density scaling exponents $\alpha = \beta = 1$

For large t , Eq. 8 has one solution for active and absorbing phases and the critical threshold $\tau = 0$

$$\rho(t) = \begin{cases} -\tau \left(g - \frac{\tau}{\rho_0}\right)^{-1} e^{\tau t}, & \text{if } \tau < 0 \\ (\rho_0^{-1} + gt)^{-1}, & \text{if } \tau = 0 \\ \frac{\tau}{g} + \frac{\tau}{g^2} \left(g - \frac{\tau}{\rho_0}\right) e^{-\tau t}, & \text{if } \tau > 0 \end{cases} \quad (9)$$

where as t grows, ρ approaches zero for $\tau \leq 0$ and $\rho \rightarrow \tau/g$ for the $\tau > 0$, i.e. asymptotically

$$\rho(t) \propto t^{-1}, \text{ if } \tau = 0 \quad (10)$$

and

$$\rho_{stat}(\tau) \propto \tau^1, \text{ if } \tau > 0. \quad (11)$$

which leads to

$$\alpha = \beta = 1. \quad (12)$$

Rapidity-reversal symmetry $\beta' = \beta$

The fact that survival of a component is measured using out-component of events in the event graph while occupation density is calculated by measuring in-component of all possibly infected nodes, hints at a symmetry in the system under time reversal. Consider δt -constrained event graph representation of temporal network $T(\mathcal{V}, \mathcal{E})$ and two sets events in bands of time δt units of time wide, namely $E_0 = \{e \in \mathcal{E} \mid 0 \leq t_e < \delta t\}$ and $E_t = \{e \in \mathcal{E} \mid t \leq t_e < t + \delta t\}$ where t_e is time of activation of event e . Assuming $S_t \subseteq E_t$ where each member of S_t appears in the out-component of at least one of the members of E_0 and $S_0 \subseteq E_0$ where each member of S_0 appears in the in-component of at least one of the members of E_t (which is to say, one of the members of S_t). Probability of survival at time t can be estimated as the fraction of nodes in E_0 that can reach at least a node in E_t , $P(t) \approx |S_0|/|E_0|$. Similarly, since in the homogeneous fully occupied case all the events in E_0 are occupied, the occupation density at time t can be estimated as $\rho(t) \approx |S_t|/|E_t|$.

Under reversal of time $t_e \rightarrow (t + \delta t) - t_e$ the direction of the links in the event graph will revert which in turn

causes switching of in- and out-component set of each node. In this scenario, occupation density is estimated by $\rho(t) \approx |S_0|/|E_0|$ which is the same as probability of survival in the original case. Conversely, probability of survival is estimated by $P(t) \approx |S_t|/|E_t|$ which is the same as occupation density in the original case. If the time-reverted event graph has the same likelihood as the original event graph, e.g. if $\mathcal{G}_0^{out} = \mathcal{G}_0^{in}$, this leads to the identity

$$P(t) = \rho(t), \quad (13)$$

which in turn, for models belonging to the DP class, leads to the celebrated rapidity-reversal symmetry:

$$\beta = \beta'. \quad (14)$$

Mean component mass exponent $\gamma = 1$

The generating function for distribution of out-component sizes $H_0(y)$ is the solution to the system

$$\begin{aligned} H_0(y) &= y \mathcal{G}_0^{out}(H_1(y)) \\ H_1(y) &= y \mathcal{G}_1^{out}(H_1(y)) \end{aligned} \quad (15)$$

and mean out-component size can be calculated as

$$M = \left. \frac{\partial H_0(y)}{\partial y} \right|_{y=1} = 1 + \mathcal{G}_0'^{out}(1) H_1'(1). \quad (16)$$

For $\tau < 0$ where $H_1(1) = 1$ this results in a solution in form of

$$\begin{aligned} H_1'(1) &= 1 + \mathcal{G}_1'^{out}(1) H_1'(1) = (1 - \mathcal{G}_1'^{out}(1))^{-1} \\ \rightarrow M &= 1 + \mathcal{G}_0'^{out}(1) (1 - \mathcal{G}_1'^{out}(1))^{-1}. \end{aligned} \quad (17)$$

Keeping in mind the definition of control parameter $\tau = \langle Q_{out} \rangle - 1 = \mathcal{G}_1'^{out}(1) - 1$ and that $\frac{\partial}{\partial y} \mathcal{G}_0^{out}(y)|_{y=1} = z$ (see Eq. 7), we can re-write M as

$$M = 1 + z(-\tau)^{-1} = \frac{z - \tau}{-\tau}, \quad (18)$$

For the special case of random k -regular networks we can prove that $z - \tau = 1$ which give the result $M = (-\tau)^{-1}$. More generally, to find exponent of a power-law asymptote of the form $(-\tau)^{-\gamma}$ as $\tau \rightarrow 0^-$ for any random graph we can find the solution to

$$\begin{aligned} -\gamma &= \lim_{\tau \rightarrow 0^-} \frac{\ln M}{\ln -\tau} = \lim_{\tau \rightarrow 0^-} \frac{\ln(z - \tau) - \ln -\tau}{\ln -\tau} \\ &= \lim_{\tau \rightarrow 0^-} \frac{\ln(z - \tau)}{-\tau} - 1 = -1 \text{ if } 0 < z < \infty. \end{aligned} \quad (19)$$

Under the condition that $0 < z < \infty$, the limit term is equal to zero, resulting in $\gamma = 1$. Given the fact that, assuming probability of co-occurrence of adjacent events is negligible, the maximum out-degree of the event graph is 2, if the mean out-degree is above zero at $\tau = 0$, a power relation with exponent $\gamma = 1$ estimates mean component mass.

ALTERNATIVE ANALOGUE FOR MEAN CLUSTER MASS

In classic DP, mean cluster mass M is defined as the integration of the pair-connectedness function across all nodes and time. Based on how we established parallels between spatial dimensions and the base networks and a the possibility of defining pair-connectedness function as existence of a δt -limited time-respecting path between a pair of nodes at different times, this might translates more directly to the sum of time-length of all infections started from a random event, or in other words total duration of sickness for all people. This would also imply that the spreading processes start at random nodes and times, as opposed to starting at random events as we use in the manuscript.

DESCRIPTION OF THE REAL-WORLD TEMPORAL NETWORK DATA SETS

Four real-world temporal networks were used for demonstrating the measurement of the quantities and phase transition. These are the same datasets used previously for developing the algorithmic method which form the backbone of the more empirical parts of the current manuscript [2].

The air transportation network dataset is a recording of 180 112 flights between 279 airports in the United States, gathered from the website of the The Department of Transportation's Bureau of Transportation Statistics website in 2017 [5]. The public transportation network is the set of all 664 138 trips during a typical Monday in Helsinki in 2018, where a trip is one public transportation vehicle moving from one of the 6 858 bus, metro and ferry stations to the next [6]. The twitter dataset is a set of 258 million mentions (counting replies) of 12 million user handles [7]. Finally, the mobile phone call dataset is set of 325 million phone calls between over 5 million mobile phone subscribers [8]. A few thousand events were removed from the beginning of the twitter dataset to eliminate a weeks-wide gap in the gathered data.

The first two networks, air and public transportation networks, were processed as directed, delayed temporal networks where each event has a duration as well as a starting time $e = (v_1, v_2, t, d)$ where two events are adjacent if the second event starts after the duration of the event is finished and the tail node of the second event is the same as the head node of the first event, e.g. the first plane lands in the destination airport before the second one takes off from that airport. The waiting time δt then refers to the time between end of the first event to the beginning of the second one.

There is an argument for measuring waiting time in delayed temporal networks from the beginning of the first

event for some processes such as disease spreading. For example, a disease that gets healed less than an hour after infecting someone has a very low chance of spreading through air travel where most trips take longer than that. That method was not used in this manuscript. The second pair of networks, twitter and mobile networks, were treated like undirected, instantaneous temporal networks.

The real-world networks show high degrees of temporal heterogeneity, daily/weekly patterns, peaks at special hours of the day or at special days of the year or local or global outages. Measuring representative values for static density ρ_{stat} and susceptibility χ for real-world networks would need special consideration. Our current method for measuring these quantities in the homogeneous, fully-occupied initial condition is dependent on the level of activity of the initial time t_0 of the dataset as well as existence of unlikely periods of very low or very high activity as a result of natural disasters, real-world happenings or simply failure of the measurement apparatus or the measured system. To average out any such outliers we split the original data into 64 equal time windows of time $T/2$ (for air and public transport) and $T/16$ (for mobile and twitter) where T is the time window of the original dataset, each starting at a random point in time.

Distribution of mass, volume and lifetime for each event in the event graph can be seen Figs. 2, 3, 4 and 5 for Helsinki public transport, Air transport, Twitter and Mobile datasets respectively.

-
- [1] A. Mellor, The temporal event graph, *Journal of Complex Networks* **6**, 639 (2017).
 - [2] A. Badie-Modiri, M. Karsai, and M. Kivelä, Efficient limited-time reachability estimation in temporal networks, *Phys. Rev. E* **101**, 052303 (2020).
 - [3] A. Badie-Modiri, A. K. Rizi, M. Karsai, and M. Kiveä, Directed percolation in random temporal network models with heterogeneities (2021), (in preparation).
 - [4] M. E. Newman, S. H. Strogatz, and D. J. Watts, Random graphs with arbitrary degree distributions and their applications, *Physical review E* **64**, 026118 (2001).
 - [5] Bureau of Transportation Statistics, (2017).
 - [6] R. Kujala, C. Weckström, R. K. Darst, M. N. Mladenović, and J. Saramäki, A collection of public transport network data sets for 25 cities, *Scientific data* **5**, 180089 (2018).
 - [7] J. Yang and J. Leskovec, Patterns of temporal variation in online media, in *Proceedings of the fourth ACM international conference on Web search and data mining* (ACM, 2011) pp. 177–186.
 - [8] M. Karsai, M. Kivelä, R. K. Pan, K. Kaski, J. Kertész, A.-L. Barabási, and J. Saramäki, Small but slow world: How network topology and burstiness slow down spreading, *Physical Review E* **83**, 025102(R) (2011).

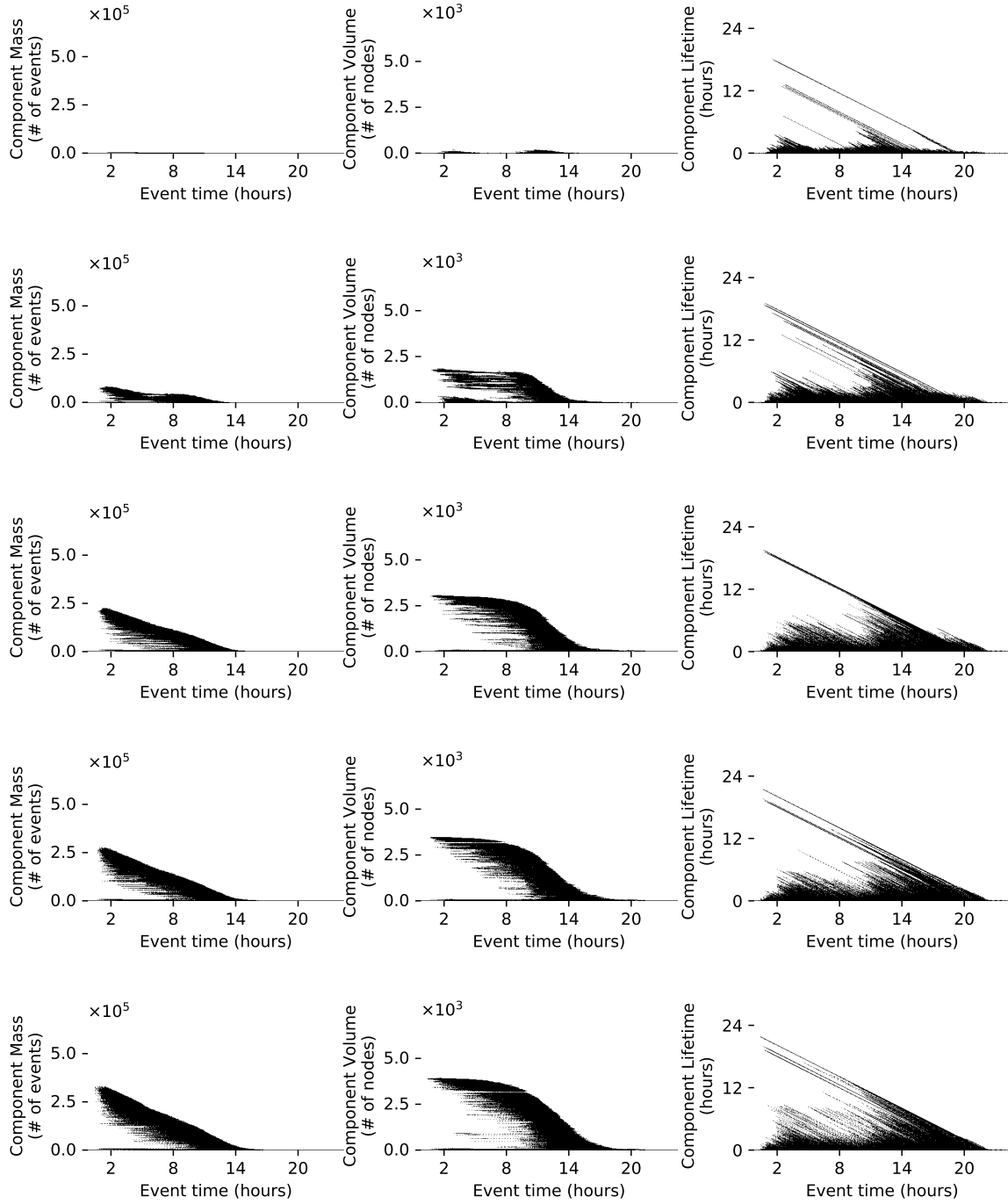


FIG. 2. Helsinki public transport network out-component size estimates for (a) $\delta t = 300$, (b) $\delta t = 500$, (c) $\delta t = \delta t_c = 670$, (d) $\delta t = 800$ and (e) $\delta t = 1000$ seconds.

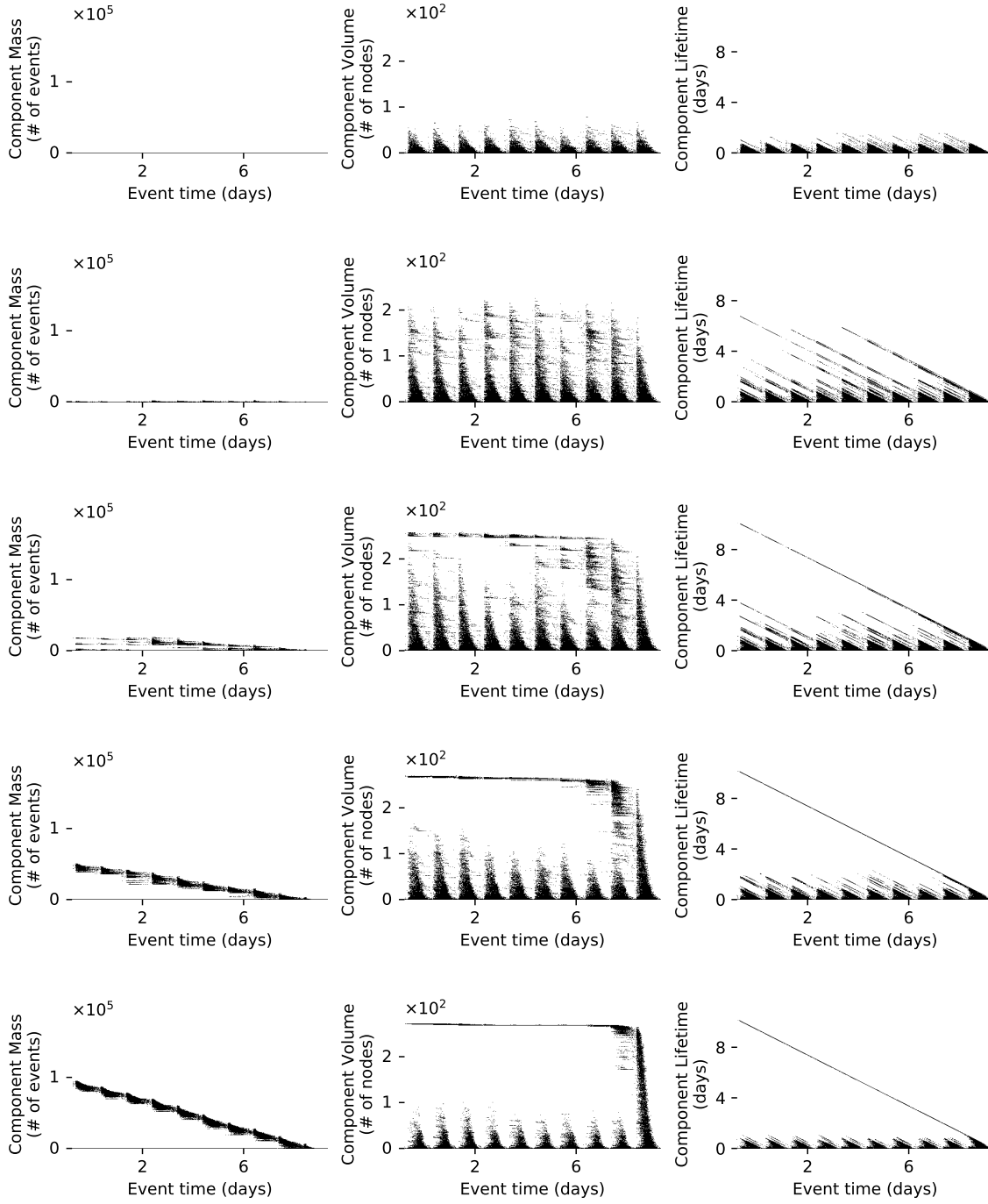


FIG. 3. Air transport network out-component size estimates for (a) $\delta t = 300$, (b) $\delta t = 400$, (c) $\delta t = \delta t_c = 470$, (d) $\delta t = 600$ and (e) $\delta t = 800$ seconds.

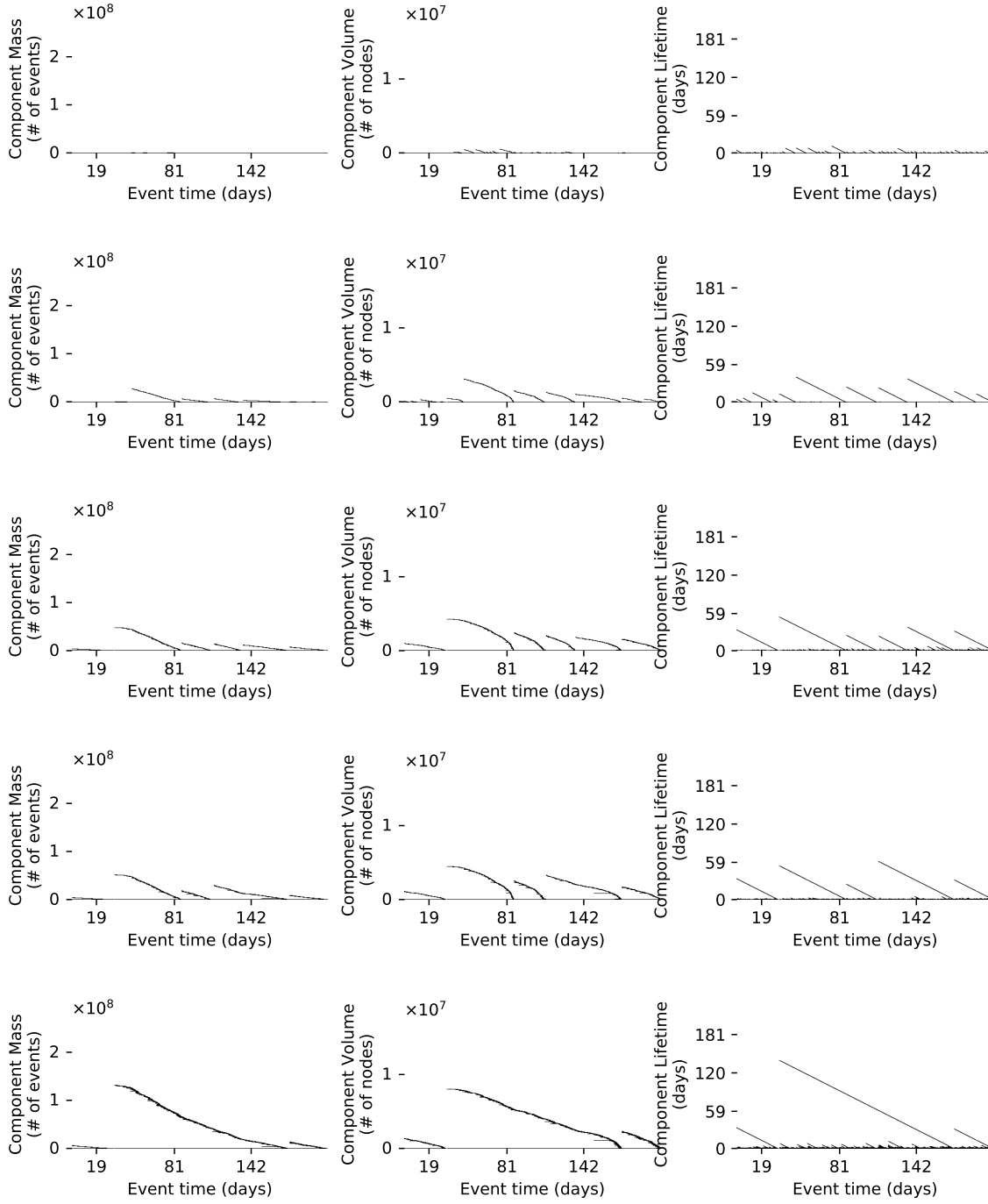


FIG. 4. Twitter mention network out-component size estimates for (a) $\delta t = 200$, (b) $\delta t = 1200$, (c) $\delta t = 3600$, (d) $\delta t = \delta t_c = 4800$ and (e) $\delta t = 12000$ seconds.

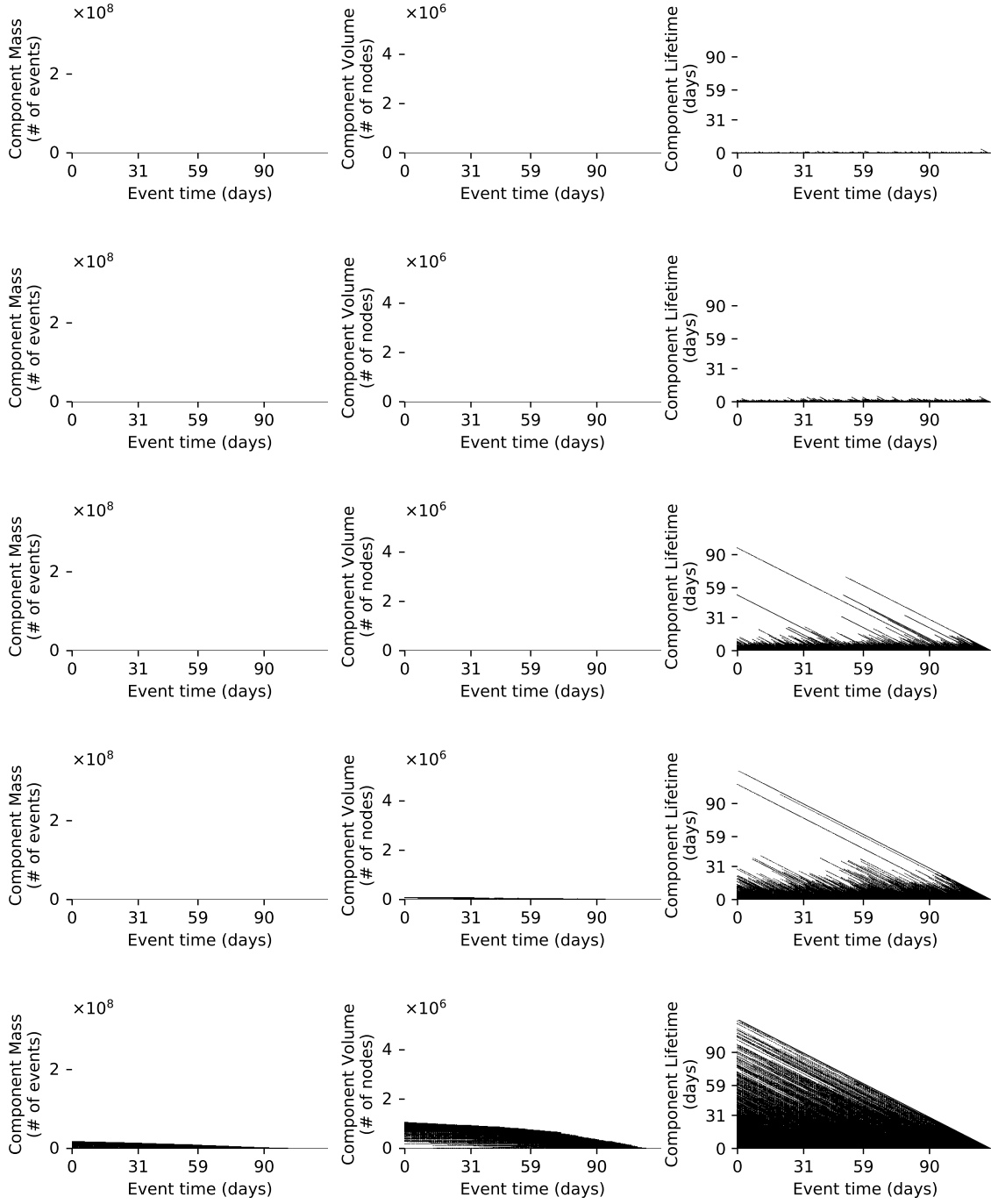


FIG. 5. Mobile call network out-component size estimates for (a) $\delta t = 2$, (b) $\delta t = 4$, (c) $\delta t = \delta t_c = 7.5$, (d) $\delta t = 9$ and (e) $\delta t = 14$ hours.